Preprint Cambridge Centre for Computational Chemical Engineering ISSN 1473 – 4273

Comparison of the Stochastic Fields method and DQMoM-IEM as turbulent reaction closures

Jethro Akroyd, Alastair J. Smith,

Laurence R. McGlashan, Markus Kraft[1]

released: 23 March 2010

[1] Department of Chemical Engineering
and Biotechnology
University of Cambridge
New Museums Site
Pembroke Street
Cambridge, CB2 3RA
United Kingdom
E-mail: mk306@cam.ac.uk

Preprint No. 95

Keywords: Mathematical modelling, Simulation, Turbulence, CFD, SF, DQMoM-IEM

Edited by
Computational Modelling Group
Department of Chemical Engineering and Biotechnology
University of Cambridge
New Museums Site
Pembroke Street
Cambridge CB2 3RA
United Kingdom

Fax: + 44 (0)1223 334796
E-Mail: c4e@cam.ac.uk
World Wide Web: http://como.ceb.cam.ac.uk/

Abstract

This paper compares two mean reaction rate closures for turbulent reacting flow: the Stochastic Fields (SF) method and the Direct Quadrature Method of Moments using the Interaction by Exchange with the Mean micromixing model (DQMoM-IEM). The methods have many common features and have received significant attention in recent literature, yet have not been systematically compared. We present both methods in the same mathematical framework and compare their numerical performance. In addition, we introduce antithetic sampling as a variance reduction technique to increase the efficiency of the SF algorithm. We extend the methodology to take advantage of this development and show details of the implementation of each method in an existing computational fluid dynamics code. We present a systematic investigation and consider both axisymmetric and 3D formulations of a problem known from the literature. DQMoM-IEM showed excellent agreement with experimental and transported probability density function data. SF gave reasonable agreement, but retained a minor grid-dependence not seen with DQMoM-IEM and did not fully resolve the sub-grid segregation of the species. The antithetic sampling was demonstrated to significantly increase the efficiency of the axisymmetric SF cases.

Contents

1 Introduction **3**

2 Theoretical background **4**

2.1 DQMoM-IEM 4

2.2 SF 5

2.3 Common features 6

3 Numerical details **7**

3.1 DQMoM-IEM coupling to CFD 7

3.2 SF coupling to CFD 8

3.3 Antithetic sampling 9

4 Comparison of DQMoM-IEM and SF **10**

4.1 Model problem 10

4.2 Application to scalar mixing 11

4.3 Application to reacting flow 15

5 Conclusions **19**

Nomenclature **20**

References **22**

Citation Index **26**

A SF derivation **27**

1 Introduction

Turbulent reacting flows are a key field of research for many engineering applications. For example, the production of titanium dioxide from titanium tetrachloride and oxygen. Current turbulent flow methods separate the velocity and scalar quantities (such as species concentration) into resolved and unresolved components. For example, Reynolds-Averaged Navier Stokes (RANS) methods solve transport equations for average components, but need to close terms arising from unresolved fluctuating components. In reacting flows, the *chemical source terms* that occur in the material and energy balance equations are left unclosed and must be modelled.

Many approaches to modelling turbulent reacting flow have been studied [9, 29, 34]. Transported probability density function (PDF) methods [22] are applicable to all flows and offer the key advantage that the chemical source term does not need to be closed. However, Monte Carlo solution techniques are typically required [35]. These may be computationally expensive and not necessarily suited to the computational fluid dynamics (CFD) software that would often be the method of choice for turbulent flow simulations.

Two methods considered in recent literature and amenable to implementation within existing CFD codes are the Direct Quadrature Method of Moments using the Interaction by Exchange with the Mean micromixing model (DQMoM-IEM) and the Stochastic Fields (SF) method. Despite the attention, no studies have directly compared the methods.

The application of DQMoM-IEM to turbulent reacting flows was suggested by Fox [9]. A weighted particle system and the interaction by exchange with the mean (IEM) [43] micromixing model are used to approximate a joint composition PDF transport equation. An arbitrary moment set is used to derive transport equations for the weights and weighted positions of the particle system that guarantee to reproduce the correct transport of the moments within this set. The method has been applied to reactive precipitation in non-ideal plug flow reactors [44], nano-particle precipitation in confined impinging jet reactors [14, 15, 30, 36] and stabilised turbulent methane-hydrogen flames [39].

The SF method [37, 42] approximates a joint composition PDF transport equation using a set of Eulerian 'stochastic fields'. The fields are defined over the entire spatial domain and evolve according to a stochastic partial differential equation (SPDE) such that they remain statistically equivalent to a one-point joint composition PDF. The method has been applied to a number of turbulent reacting flows including the dispersion of reactive pollutants [12, 13], piloted methane flames [32], and the auto-ignition of hydrogen and n-heptane flames [23–25].

The **purpose of this paper** is to compare the numerical behaviour of DQMoM-IEM and SF and to introduce antithetic sampling to improve the SF method. Section 2 introduces the key aspects of each method. Section 3 summarises the implementation of DQMoM-IEM and SF and explains the use of antithetic sampling to increase the efficiency of the SF simulations. Section 4 investigates the performance of DQMoM-IEM and SF against the method of moments and a turbulent reaction test case known from the literature [28, 40, 41]. Both axisymmetric and 3D cases are considered. The benefits of antithetic sampling are discussed and areas for further research suggested.

2 Theoretical background

This section introduces key aspects of the DQMoM-IEM and SF methods and discusses some common features. The derivations of the methods are documented in the literature and solve approximations to a closed joint composition PDF transport equation such as

$$\begin{aligned}\frac{\partial f_\phi}{\partial t} + \langle U_i \rangle \frac{\partial f_\phi}{\partial x_i} - \frac{\partial}{\partial x_i}\left(\Gamma_\mathrm{T} \frac{\partial f_\phi}{\partial x_i}\right) = \\ - \frac{\partial}{\partial \psi_\alpha}\left(\left[\frac{C_\phi}{2\tau_\phi}\left(\langle \phi_\alpha \rangle - \psi_\alpha\right) + S_\alpha(\psi)\right] f_\phi\right).\end{aligned} \tag{1}$$

2.1 DQMoM-IEM

DQMoM-IEM was first derived by Fox [9, Appendix B]. Its numerical implementation as a turbulent reaction closure has been investigated in detail by Akroyd et al. [2].

This paper considers the case when the closed joint composition PDF transport equation (1) is approximated using a weighted particle system

$$\begin{aligned} f_\phi(\psi; x, t) &= f_\phi(\psi_1, \psi_2, \ldots, \psi_K; x, t) \\ &\approx \sum_{n=1}^{N} w^{(n)}(x,t) \prod_{\alpha=1}^{K} \delta_{\psi_\alpha^{(n)};x,t}\,, \end{aligned} \tag{2}$$

where

$$\delta_{\psi_\alpha^{(n)};x,t} \equiv \delta\left[\psi_\alpha - \psi_\alpha^{(n)}(x,t)\right]. \tag{3}$$

The particle system introduces N weights $w^{(n)}$ and NK positions $\psi_\alpha^{(n)}$, where $n = 1, \ldots, N$ particles and $\alpha = 1, \ldots, K$ scalars.

Transport equations that share the form of standard scalar transport equations are derived for the weights $w^{(n)}$ and weighted positions $s_\alpha^{(n)}$ of the particle system

$$\frac{\partial w^{(n)}}{\partial t} + \langle U_i \rangle \frac{\partial w^{(n)}}{\partial x_i} - \frac{\partial}{\partial x_i}\left(\Gamma_\mathrm{T} \frac{\partial w^{(n)}}{\partial x_i}\right) = a^{(n)}\,, \tag{4}$$

$$\frac{\partial s_\alpha^{(n)}}{\partial t} + \langle U_i \rangle \frac{\partial s_\alpha^{(n)}}{\partial x_i} - \frac{\partial}{\partial x_i}\left(\Gamma_\mathrm{T} \frac{\partial s_\alpha^{(n)}}{\partial x_i}\right) = b_\alpha^{(n)}\,, \tag{5}$$

where

$$s_\alpha^{(n)} \equiv w^{(n)} \psi_\alpha^{(n)}\,. \tag{6}$$

The source terms $a^{(n)}$ are set to zero and the weights evolve as conserved scalars subject to equation (4). A set of $M = NK$ unmixed empirical moments

$$\langle \phi_\alpha^{m_{\lambda\alpha}} \rangle_N = \sum_{n=1}^{N} w^{(n)} \psi_\alpha^{(n)m_{\lambda\alpha}} \qquad \text{for } \lambda = 1, \ldots, M\,, \tag{7}$$

are used to derive a linear system of NK equations for the source terms $b_\alpha^{(n)}$. In the case that the unmixed empirical moments are specified

$$m_{\lambda\alpha} = \lambda \qquad \text{for } \lambda = 1, \ldots, N \text{ and } \alpha = 1, \ldots, K\,, \tag{8}$$

the linear system can be solved to give a set of N equations for each scalar $\alpha = 1, \ldots, K$ [2]

$$b_\alpha^{(n)} = b_{\mathrm{mx}_\alpha}^{(n)} + b_{\mathrm{rx}_\alpha}^{(n)} + b_{\mathrm{dx}_\alpha}^{(n)}\,, \tag{9}$$

where

$$b_{\mathrm{mx}_\alpha}^{(n)} = w^{(n)} \frac{C_\phi}{2\tau_\phi} \left(\langle \phi_\alpha \rangle_N - \psi_\alpha^{(n)} \right), \tag{10}$$

$$b_{\mathrm{rx}_\alpha}^{(n)} = w^{(n)} S_\alpha \left(\psi^{(n)} \right), \tag{11}$$

$$\begin{aligned} b_{\mathrm{dx}_\alpha}^{(n)} = {} & w^{(n)} c_{\alpha\alpha}^{(n)} \sum_{\substack{i=1 \\ i\neq n}}^{N} \frac{1}{\psi_\alpha^{(n)} - \psi_\alpha^{(i)}} \\ & + \prod_{\substack{i=1 \\ i\neq n}}^{N} \frac{1}{\psi_\alpha^{(n)} - \psi_\alpha^{(i)}} \sum_{\substack{j=1 \\ j\neq n}}^{N} w^{(j)} c_{\alpha\alpha}^{(j)} \prod_{\substack{k=1 \\ k\neq j,n}}^{N} \left(\psi_\alpha^{(j)} - \psi_\alpha^{(k)} \right), \end{aligned} \tag{12}$$

and

$$c_{\alpha\beta}^{(n)} \equiv \Gamma_{\mathrm{T}} \frac{\partial \psi_\alpha^{(n)}}{\partial x_i} \frac{\partial \psi_\beta^{(n)}}{\partial x_i}\,. \tag{13}$$

The $b_{\mathrm{mx}_\alpha}^{(n)}$ and $b_{\mathrm{rx}_\alpha}^{(n)}$ terms describe micromixing and chemical reaction, $b_{\mathrm{dx}_\alpha}^{(n)}$ describes the effect of turbulent diffusion in the presence of spatial gradients of scalar α. We refer to them as the DQMoM-IEM *micromixing*, *reaction* and *diffusion* terms.

2.2 SF

The SF method was derived independently by Valiño [42] and Sabel'nikov and Soulard [37]. The derivations differ in that Valiño derives an Itô SPDE under the restriction that the fields are twice differentiable in space, whereas Sabel'nikov and Soulard present a more general derivation of a Stratonovich SPDE and show equivalence to Valiño's result.

This paper considers the case of a multivariate Itô SPDE, first given by Hauke and Valiño [21]. The derivation follows the approach outlined by Valiño [42] and is summarised in the appendix for the benefit of readers who would appreciate more detail. The joint composition PDF transport equation (1) is approximated using an ensemble of N fields

$$\begin{aligned} f_\phi(\psi; x, t) &= f_\phi(\psi_1, \psi_2, \ldots, \psi_K; x, t) \\ &\approx \frac{1}{N} \sum_{n=1}^{N} \prod_{\alpha=1}^{K} \delta_{\psi_\alpha^{(n)};x,t}\,, \end{aligned} \tag{14}$$

where $\delta_{\psi_\alpha^{(n)};x,t}$ is defined as per equation (3). Hauke and Valiño [21] state the equivalent SPDE describing the transport of each field $\psi_\alpha^{(n)}(x,t)$

$$\begin{aligned} \mathrm{d}\psi_\alpha^{(n)} = &- \langle U_i \rangle \frac{\partial \psi_\alpha^{(n)}}{\partial x_i}\,\mathrm{d}t + \frac{\partial}{\partial x_i}\left(\Gamma_\mathrm{T} \frac{\partial \psi_\alpha^{(n)}}{\partial x_i}\right)\mathrm{d}t \\ &+ \frac{C_\phi}{2\tau_\phi}\left(\langle \phi_\alpha \rangle_N - \psi_\alpha^{(n)}\right)\mathrm{d}t + S_\alpha\left(\psi^{(n)}\right)\mathrm{d}t \\ &+ \left(2\Gamma_\mathrm{T}\right)^{1/2} \frac{\partial \psi_\alpha^{(n)}}{\partial x_i}\,\mathrm{d}W_i^{(n)}\,, \end{aligned} \tag{15}$$

where W is a Wiener process, see Gardiner [10]. The final three terms describe micromixing, chemical reaction and the effect of turbulent diffusion in the presence of spatial gradients of scalar α. We refer to them as the SF *micromixing*, *reaction* and *diffusion* terms.

2.3 Common features

DQMoM-IEM and SF have many common features. Both invoke the same approximation to discretise the closed joint composition PDF transport equation (1) in composition space. The weighted particle system in equation (2) is a field approximation analogous to that introduced by the SF method in equation (14). In the case that DQMoM-IEM is constrained $w^{(n)} = 1/N$, equation (5) may be rewritten in terms of $\psi_\alpha^{(n)}$ in an analogous form to the SF equation (15), where the equations differ only in their treatment of the DQMoM-IEM and SF diffusion terms.

In DQMoM-IEM, the moments of the modelled PDF are governed by the particle weights and positions. The method is deterministic and typically only a few particles are required. In particular, it is the correct specification of the boundary conditions on the weights that allows the underlying PDF to be modelled with only a few particles [2]. In the case of SF, the method specifies equi-weighted fields, and the moments of the modelled PDF are governed entirely by the stochastic action of equation (15). In contrast to DQMoM-IEM, the implementation is simplified at the cost of requiring a larger number of fields both to resolve the modelled PDF and to control statistical error.

3 Numerical details

This section presents the numerical details of the DQMoM-IEM and SF implementations. Sections 3.1 and 3.2 describe the coupling of each method to the Star-CD CFD code [5]. Section 3.3 introduces the application of antithetic sampling to improve the statistical efficiency of the SF implementation.

3.1 DQMoM-IEM coupling to CFD

DQMoM-IEM is coupled to Star-CD using an operator splitting technique and solved as a transient problem, where $w^{(n)}$ and $s_\alpha^{(n)}$ are implemented as passive scalars. The method is described in detail by Akroyd et al. [2] and is summarised below.

Equation (4) is solved using Star-CD. Equation (5) is solved using a Strang [38] splitting

$$\frac{\partial s_\alpha^{(n)}}{\partial t} = -\left\langle U_i \right\rangle \frac{\partial s_\alpha^{(n)}}{\partial x_i} + \frac{\partial}{\partial x_i}\left(\Gamma_\mathrm{T} \frac{\partial s_\alpha^{(n)}}{\partial x_i}\right), \tag{16}$$

$$\frac{\partial s_\alpha^{(n)}}{\partial t} = b_\alpha^{(n)}, \tag{17}$$

where equation (16) is solved using Star-CD with time step Δt, and equation (17) is solved with time step $\frac{1}{2}\Delta t$ before the first and after the last iteration, and time step Δt otherwise.

The numerical treatment of equation (17) requires special care to avoid discontinuities and enforce boundedness. It is solved using one of either the *analytic* or *general* solver methods described by Akroyd et al. [2]. The particular implementations in this paper invoke a further splitting given for the analytic solver

$$S_{\Delta t}^{b_\alpha^{(n)}}\left(s_\alpha^{(n)}\right) \approx \left[S_{\frac{1}{2}\Delta t}^{b_{\mathrm{mx}\alpha}^{(n)}} \circ S_{\frac{1}{2}\Delta t}^{b_{\mathrm{dx}\alpha}^{(n)}} \circ S_{\Delta t}^{b_{\mathrm{rx}\alpha}^{(n)}} \circ S_{\frac{1}{2}\Delta t}^{b_{\mathrm{dx}\alpha}^{(n)}} \circ S_{\frac{1}{2}\Delta t}^{b_{\mathrm{mx}\alpha}^{(n)}}\right]\left(s_\alpha^{(n)}\right), \tag{18}$$

and the general solver

$$S_{\Delta t}^{b_\alpha^{(n)}}\left(s_\alpha^{(n)}\right) \approx \left[S_{\frac{1}{2}\Delta t}^{b_{\mathrm{mx}\alpha}^{(n)}+b_{\mathrm{dx}\alpha}^{(n)}} \circ S_{\Delta t}^{b_{\mathrm{rx}\alpha}^{(n)}} \circ S_{\frac{1}{2}\Delta t}^{b_{\mathrm{mx}\alpha}^{(n)}+b_{\mathrm{dx}\alpha}^{(n)}}\right]\left(s_\alpha^{(n)}\right), \tag{19}$$

where $S_{\Delta t}$ denotes the solution operator

$$S_{\Delta t}^{b_\alpha^{(n)}}\left(s_\alpha^{(n)}\right) \;:\; s_\alpha^{(n)}(t) \mapsto s_\alpha^{(n)}(t+\Delta t)\,.$$

The numerical integration of the reaction and the general solver micromixing-diffusion terms is performed using RADAU5 [17].

3.2 SF coupling to CFD

SF is coupled to Star-CD using the same method as DQMoM-IEM. The fields $\psi_\alpha^{(n)}(x,t)$ are implemented as passive scalars. Equation (15) is solved using a Strang [38] splitting

$$\mathrm{d}\psi_\alpha^{(n)} = -\langle U_i \rangle \frac{\partial \psi_\alpha^{(n)}}{\partial x_i}\,\mathrm{d}t + \frac{\partial}{\partial x_i}\left(\Gamma_\mathrm{T}\frac{\partial \psi_\alpha^{(n)}}{\partial x_i}\right)\mathrm{d}t\,, \tag{20}$$

$$\mathrm{d}\psi_\alpha^{(n)} = \frac{C_\phi}{2\tau_\phi}\left(\langle\phi_\alpha\rangle_N - \psi_\alpha^{(n)}\right)\mathrm{d}t + S_\alpha\left(\psi^{(n)}\right)\mathrm{d}t + \left(2\Gamma_\mathrm{T}\right)^{1/2}\frac{\partial \psi_\alpha^{(n)}}{\partial x_i}\,\mathrm{d}W_i^{(n)}\,, \tag{21}$$

where equation (20) is solved using Star-CD and equation (21) is further split

$$\psi_\alpha^{(n)\dagger_1} = \psi_\alpha^{(n)}(t) + \int_0^{\frac{1}{2}\Delta t}\frac{C_\phi}{2\tau_\phi}\left(\langle\phi_\alpha\rangle_N - \psi_\alpha^{(n)}\right)\mathrm{d}\tau\,, \quad \psi_\alpha^{(n)} = \psi_\alpha^{(n)}(t) \text{ at } \tau = 0\,, \tag{22}$$

$$\psi_\alpha^{(n)\dagger_2} = \psi_\alpha^{(n)\dagger_1} + \int_0^{\Delta t}\left(2\Gamma_\mathrm{T}\right)^{1/2}\frac{\partial \psi_\alpha^{(n)}}{\partial x_i}\,\mathrm{d}W_i^{(n)}\,, \quad \psi_\alpha^{(n)} = \psi_\alpha^{(n)\dagger_1} \text{ at } \tau = 0\,, \tag{23}$$

$$\psi_\alpha^{(n)\dagger_3} = \psi_\alpha^{(n)\dagger_2} + \int_0^{\Delta t} S_\alpha\left(\psi^{(n)}\right)\mathrm{d}\tau\,, \quad \psi_\alpha^{(n)} = \psi_\alpha^{(n)\dagger_2} \text{ at } \tau = 0\,, \tag{24}$$

$$\psi_\alpha^{(n)}(t+\Delta t) = \psi_\alpha^{(n)\dagger_3} + \int_0^{\frac{1}{2}\Delta t}\frac{C_\phi}{2\tau_\phi}\left(\langle\phi_\alpha\rangle_N - \psi_\alpha^{(n)}\right)\mathrm{d}\tau\,, \quad \psi_\alpha^{(n)} = \psi_\alpha^{(n)\dagger_3} \text{ at } \tau = 0\,. \tag{25}$$

Equation (24) is solved using RADAU5 to integrate the reaction term as per DQMoM-IEM. Equations (22) and (25) are solved analytically [3, 27]. Equation (23) is solved over the whole time step Δt, as opposed to splitting it either side of the reaction operator, in order to maintain the required independence between the integrand and $\mathrm{d}W_i^{(n)}$ [10]. It is solved following Garmory [11], using the Euler-Maruyama approximation of an Itô process [26] to solve the SF diffusion term

$$\psi_\alpha^{(n)\dagger_2} = \psi_\alpha^{(n)\dagger_1} + \left(2\Gamma_\mathrm{T}\right)^{1/2}\frac{\partial \psi_\alpha^{(n)\dagger_1}}{\partial x_i}\Delta W_i^{(n)}\,, \tag{26}$$

where

$$\Delta W_i^{(n)} = \xi_i^{(n)}(\Delta t)^{1/2}\,, \tag{27}$$

$$\xi_i^{(n)} \sim \mathcal{N}(0,1)\,. \tag{28}$$

The variates $\xi_i^{(n)}$ are independent for each spatial dimension and field, but common for all scalars α relating to dimension i and field n. They are generated using the method of Ahrens and Dieter [1], with uniform variates supplied by the Mersenne Twister MT19937 algorithm [31] with a fixed seed. This implementation may lead to loss of boundedness [11]. We therefore bound the fields after the Wiener step as per DQMoM-IEM [2].

3.3 Antithetic sampling

Antithetic sampling is a variance reduction technique. It was introduced by Hammersley and Morton [20] to increase the efficiency of Monte Carlo simulations, where the efficiency is defined in terms of the effort required to achieve a given reduction in statistical error. The premise of the method is that the variance between repetitions of a Monte Carlo simulation is reduced by introducing pair-wise negative correlation between replicates.

The mathematical basis for antithetic sampling is defined in work led by Hammersley [18–20] and Wilson [45, 46], and summarised by Fishman [7]. The method has mostly been applied within quantitative economics [16] and finance [4, 33]. Its application within computer simulations has been investigated by Cheng [6] and Fishman and Huang [8].

We apply antithetic sampling to the SF method, treating each field as a replicate. The idea is to increase the efficiency, such that a given result can be achieved with fewer fields and without necessarily requiring repetition of the entire simulation. We sample the variates for odd-numbered fields, but prescribe them for even-numbered fields

$$\xi_i^{(n)} \sim \mathcal{N}(0,1) \text{ if } n \in 2\mathbb{N}+1\,, \quad \xi_i^{(n)} = -\xi_i^{(n-1)} \text{ if } n \in 2\mathbb{N}\,. \tag{29}$$

This is the *reflection sampling* method described by Fishman and Huang [8] and the 'standard' method used as the basis for the investigation by Cheng [6]. Cheng suggests several possible refinements, but we restrict our attention to the method defined by equation (29) for the purposes of this initial investigation.

The rest of this paper compares the performance of DQMoM-IEM and SF, and considers the impact of antithetic sampling. We denote SF cases with sampling as per equation (28) as *standard cases*, and those with sampling as per equation (29) as *antithetic cases*. We note that in this implementation and for a given number of iterations, a standard case with N fields would use the same sequence of variates as the first half of a standard case or a full antithetic case with $2N$ fields.

4 Comparison of DQMoM-IEM and SF

This section investigates the performance of the DQMoM-IEM and SF methods described in Section 3 against a test case known from the literature.

Section 4.1 describes the test case. Section 4.2 assesses the performance of DQMoM-IEM and SF against the method of moments. This enables the effect of the numerical implementation of the diffusion terms described in Sections 2 and 3 to be examined in isolation. Section 4.3 compares the application of both methods to a reacting system.

4.1 Model problem

The investigations in this paper were performed using a constant density test case, selected because it has been well studied numerically [40] and experimentally [28]. The system considered is the isothermal liquid-phase reaction

$$\mathrm{A} + \mathrm{B} \xrightarrow{k_1} \mathrm{R}, \ \mathrm{B} + \mathrm{R} \xrightarrow{k_2} \mathrm{S}\,, \tag{30}$$

$k_1 = 5.0 \times 10^6$ m^3/kmol s, $k_2 = 1.8 \times 10^3$ m^3/kmol s. The yield of R

$$Y = \frac{C_\mathrm{R}}{C_\mathrm{R} + 2C_\mathrm{S}}\,, \tag{31}$$

is sensitive to the rate of mixing due to the difference in the magnitude of the rate constants. The case offers a simple approximation to stiff chemistry.

The reactor configuration is illustrated in **Figure 1**. It is the single-jet system previously considered during the development of the DQMoM-IEM solvers [2] used in this paper. This investigation considers the high concentration case where a turbulent jet of species B with Reynolds number Re=3530 is injected into a laminar annular coflow of species A.

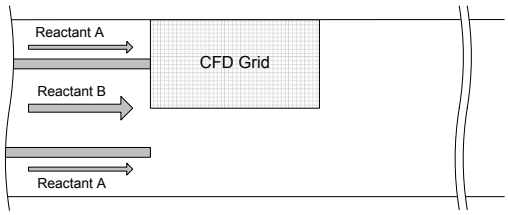

Figure 1: *Configuration of the single-jet tubular reactor.*

The system was solved using Star-CD [5] as per Akroyd et al. [2]. The inlet boundary conditions on the flow are those used previously [2, Table 1]. The composition space is defined in terms of the mass fractions

$$\phi^\top = \left[Y_\mathrm{A}, Y_\mathrm{B}, Y_\mathrm{R}, Y_\mathrm{S}, Y_\mathrm{solvent}\right], \tag{32}$$

The initial and inlet boundary conditions on the mass fractions and the DQMoM-IEM particle weights are given in **Table 1**.

Table 1: *DQMoM-IEM and SF initial and inlet boundary conditions.*

	Initial condition	Inlet boundary		
		Jet	Annulus	
$w^{(n)}$	$1/N$	0 [a]	$1/\lfloor \frac{N}{2} \rfloor$	for $n \leqslant \lfloor \frac{N}{2} \rfloor$
	$1/N$	$1/\lceil \frac{N}{2} \rceil$	0 [a]	for $n > \lfloor \frac{N}{2} \rfloor$
$\psi_{\mathrm{A}}^{(n)}$	0	0	4.27×10^{-4} [b]	
$\psi_{\mathrm{B}}^{(n)}$	0	5.25×10^{-4} [b]	0	
$\psi_{\mathrm{R,S}}^{(n)}$	0	0	0	
$\psi_{\mathrm{solvent}}^{(n)}$	1	$1 - \psi_{\mathrm{B}}^{(n)}$	$1 - \psi_{\mathrm{A}}^{(n)}$	

Note that the table specifies $\psi_\alpha^{(n)}$ for clarity, but that DQMoM-IEM transports $w^{(n)}$ and $s_\alpha^{(n)} = w^{(n)}\psi_\alpha^{(n)}$.

[a] *It is convenient to avoid zero-weighted particles. In this instance, a perturbation of 10^{-6} was applied and the weights normalised.*

[b] *A perturbation was applied to avoid equal $\psi_\alpha^{(n)}$ for DQMoM-IEM cases where $w^{(n)} \neq 0$. The perturbations preserved the mean mass fraction and ensured that the DQMoM-IEM solver did not filter the diffusion source term [see 2] at the inlet boundaries.*

The behaviour of the DQMoM-IEM and SF methods are investigated using three grids. The first is the *base* grid from Akroyd et al. [2]. This uses a wedge-shaped domain of 68×23 (axial $\times$ radial) fully structured hexahedral cells. The second is a *coarse* grid, which is a simplified version of the base grid and uses a 34×14 (axial $\times$ radial) domain. The third is a *coarse 3D* grid, which models the full reactor geometry using a cylindrical domain of $34 \times 14 \times 18$ (axial $\times$ radial $\times$ azimuthal) fully structured hexahedral cells defined in a cartesian coordinate system. All cases were solved with time step 10^{-4} s on the base grid and 10^{-3} s on the coarse grids.

The SF method has so far inhibited the use of symmetric boundary conditions, since it is not clear how they should be applied to the stochastic fields [11, 37]. However, the test case flow field is axisymmetric and the DQMoM-IEM solutions are dominated by radial gradients. We use this to justify imposing an azimuthal zero-gradient condition to enforce an axisymmetric solution on the base and coarse grids. The difference between the grids causes small differences between the solutions near the inlets. However, the data are considered to be sufficiently grid-independent based on the grid causing a variation of less than 0.3% in the yield of the DQMoM-IEM cases solved in Section 4.3 (see Table 3). The effect of the grid on the SF cases is considered in more detail in the following sections.

4.2 Application to scalar mixing

This section compares the performance of the DQMoM-IEM and SF methods for a scalar mixing case. A reference solution is provided using the method of moments. The application of the method of moments to such problems is well established and provides an exact solution to equation (1) where the chemical source term is null, $S_\alpha = 0$. This approach allows the effect of the numerical implementation of the diffusion terms described in Sections 2 and 3 to be examined in isolation from the effects of reaction.

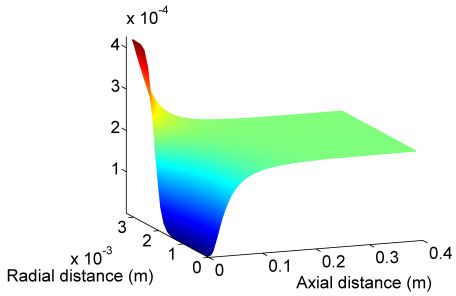

(a) *Empirical mean, species A.*

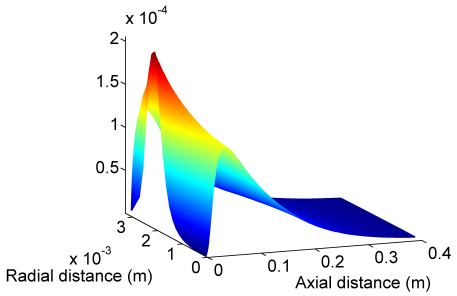

(b) *Empirical standard deviation, species A.*

Figure 2: *Jet reactor empirical mean and standard deviation of species* A *for the inert case on the base grid, DQMoM-IEM analytic solver with* $N = 2$ *particles.*

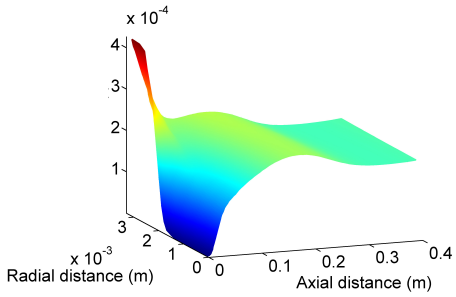

(a) *Empirical mean, species A.*

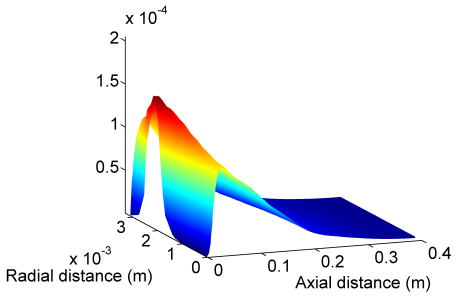

(b) *Empirical standard deviation, species A.*

Figure 3: *Jet reactor empirical mean and standard deviation of species* A *for the inert case at* $t = 5$ *s on the base grid, SF solver with standard sampling and* $N = 64$ *fields.*

Figure 2 presents the empirical mean and standard deviation of species A calculated using DQMoM-IEM. The data are visually indistinguishable from the method of moments.

Figure 3 presents corresponding data for a typical SF case. It highlights some important issues. Figure 3(a) shows a 'hump' in the mean. This is caused by the SF diffusion term where the method applies a set of variates $\xi_i^{(n)}$ that do not have exactly zero mean. This is most apparent in the radial direction because the effect of the diffusion term is dominated by the relative magnitude of the radial gradients. Such 'humps' are convected by the flow and can be observed as *fluctuations* in the values of the species means at the reactor outlet. This effect should decrease as the number of fields is increased, since the mean of the set of variates will converge in probability at a rate proportional to $N^{-1/2}$

$$\lim_{N\to\infty} \mathbb{P}\left(\left| \frac{1}{N} \sum_{n=1}^{N} \xi_i^{(n)} \right| \geqslant \varepsilon_i \right) = 0, \quad \forall \varepsilon_i > 0\,. \tag{33}$$

Figure 3(b) shows that the SF solution does not completely resolve the standard deviation near the reactor inlets. A similar observation is made using DQMoM-IEM with equi-weighted particles [2]. In this instance, DQMoM-IEM can reproduce Figure 3(b) using $N=2$ particles and boundary conditions $w_{\text{jet}}^{(1)} \approx 0.4$, $w_{\text{jet}}^{(2)} \approx 0.6$ and $w_{\text{annulus}}^{(n)} = 1 - w_{\text{jet}}^{(n)}$.

Figure 4 plots the fluctuation of the mean species B mass fraction at the reactor outlet for SF cases with $N = 4, 8, 16, 32, 64$ fields. The fluctuation is calculated

$$\max_{\substack{\text{reactor outlet} \\ t\in[1,5]\text{ s}}} \left(\langle\phi_{\mathrm{B}}\rangle_N\right) - \min_{\substack{\text{reactor outlet} \\ t\in[1,5]\text{ s}}} \left(\langle\phi_{\mathrm{B}}\rangle_N\right). \tag{34}$$

The fluctuations are calculated from time $t = 1$ s as this is the point at which DQMoM-IEM reaches steady state. Figure 4 confirms that the fluctuations converge at a rate proportional to $N^{-1/2}$ for both the standard and antithetic cases. The antithetic cases show significantly reduced fluctuation on the base and coarse grids due to the antithetic sampling enforcing a zero mean condition on the set of variates $\xi_i^{(n)}$ in each direction i. However, the fluctuations remain finite because the antithetic case does not enforce equal gradients within each antithetic pair of fields.

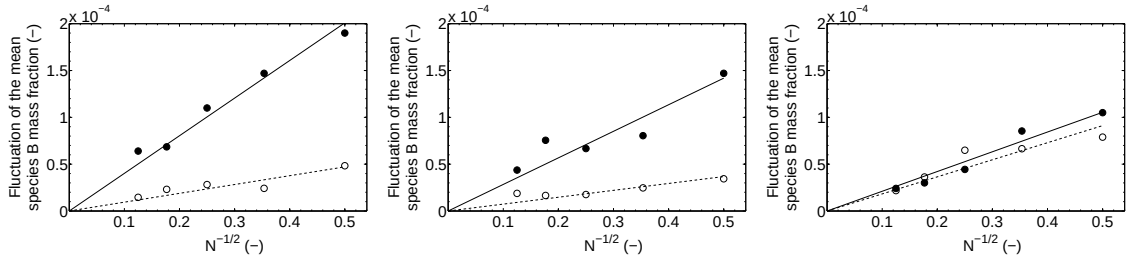

(a) *Base grid.* **(b)** *Coarse grid.* **(c)** *Coarse 3D grid.*

Figure 4: *Fluctuation of the SF mean species* B *mass fraction at the jet reactor outlet for the inert case in the interval* $t \in [1, 5]$ *s. Solid symbols: standard case; Solid line: standard case guide line; Hollow symbols: antithetic case; Dashed line: antithetic case guide line.*

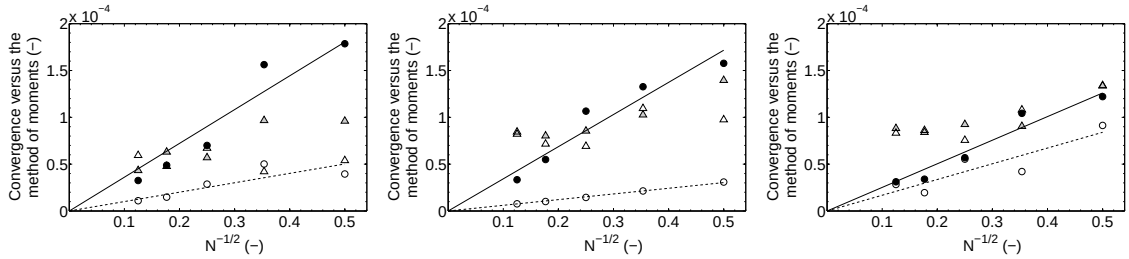

(a) *Base grid.* **(b)** *Coarse grid.* **(c)** *Coarse 3D grid.*

Figure 5: *Convergence of SF versus the method of moments for the inert case at* $t = 5$ *s. Solid symbols: standard case; Solid line: standard case guide line; Hollow symbols: antithetic case; Dashed line: antithetic case guide line. Circles (○): convergence of mean,* ϵ_{mean}*; Triangles (△): convergence of standard deviation,* ϵ_{sd}*.*

The coarse 3D grid shows little difference between the standard and antithetic cases, with fluctuations approximately two-thirds the size of those for the standard case on the coarse grid. This is less than the $\sqrt{\frac{2}{3}}$ size that might be expected by considering that the coarse grid cases use only two-thirds of the variates (the rest are multiplied by the zero azimuthal gradient). It is suggested that this is a consequence of solving the case in cartesian coordinates. The cartesian contributions to the SF diffusion term act at different angles to

the radial and azimuthal directions at different points in the radial-azimuthal plane. This gives a non-axisymmetric solution and reduces the magnitude of the fluctuations in the standard case, but undoes most of the effect of the antithetic sampling causing an increase in the antithetic case. This explanation suggests that a 3D case solved in cylindrical polar coordinates, where the radial and azimuthal contributions to the diffusion term would remain in fixed alignment with the radial and azimuthal directions, should preserve the symmetry of the solution and reproduce the results from the coarse rather than coarse 3D grid.

Figure 5 plots the convergence between SF and the method of moments. **Table 2** shows equivalent data for DQMoM-IEM. The convergence was assessed using the metrics

$$\epsilon_{\text{mean}} = \frac{1}{N_{\text{cells}}} \sum_{\alpha=1}^{K} \left\| \langle \phi_\alpha \rangle_N - \langle \phi_\alpha \rangle_N \Big|_{\text{MoM}} \right\|, \tag{35}$$

$$\epsilon_{\text{sd}} = \frac{1}{N_{\text{cells}}} \sum_{\alpha=1}^{K} \left\| \sqrt{\langle \phi_\alpha^2 \rangle_N - \langle \phi_\alpha \rangle_N^2} - \sqrt{\langle \phi_\alpha^2 \rangle_N - \langle \phi_\alpha \rangle_N^2} \Big|_{\text{MoM}} \right\|, \tag{36}$$

where the norm notation $\|\cdot\|$ denotes an L^2-norm over space. Note that Figure 5 represents a 'snapshot' of the data at $t = 5$ s, so should be expected to show more noise than Figure 4.

Figure 5 shows that ϵ_{mean} converges at a rate proportional to $N^{-1/2}$. A clear improvement is shown for the antithetic versus standard case for the base and coarse grids. Again, the coarse 3D grid shows a similar effect to that in Figure 4. The convergence is between that observed for the standard and antithetic cases on the coarse grid, with a small benefit from the antithetic case in this instance. Similar convergence is shown for ϵ_{sd} up to $N = 16$ fields, possibly with some benefit and certainly no harm from the antithetic versus standard cases. At $N > 16$ fields, ϵ_{sd} is observed to reach a steady value. The coarse grids reach $\epsilon_{\text{sd}} \approx 0.8\times10^{-4}$, whereas the base grid does slightly better at $\epsilon_{\text{sd}} \approx 0.6\times10^{-4}$. This is indicative of at least some grid dependence in the SF solution. Similar observations have been reported for DQMoM-IEM by Gavi et al. [15]. In all cases, comparison of Figure 5 with Table 2 shows that DQMoM-IEM achieves better convergence than SF.

Table 2: *Convergence of the DQMoM-IEM mean and standard deviation versus the method of moments for the inert case at $t = 2$ s.*

Grid	ϵ_{mean}			ϵ_{sd}		
	$N=2^a$	$N=2^b$	$N=3^b$	$N=2^a$	$N=2^b$	$N=3^b$
Base	6.9×10^{-7} [c]	6.9×10^{-7}	4.4×10^{-7}	4.7×10^{-6} [c]	4.7×10^{-6}	4.8×10^{-6}
Coarse	6.5×10^{-7}	–	–	2.9×10^{-6}	–	–
3D coarse	6.5×10^{-7}	–	–	4.5×10^{-6}	–	–

[a] *Analytic solver [2],* [b] *General solver [2],* [c] *See Figure 2.*

4.3 Application to reacting flow

This section compares the application of the DQMoM-IEM and SF methods presented in Section 3 to previous studies [2, 28, 40] of a real turbulent reaction problem.

Table 3 summarises the yields for all DQMoM-IEM cases considered and shows good agreement with the previous studies [28, 40]. In particular, the agreement is improved over previous cases [2] due to the inclusion of the solvent component, see equation (32).

Figures 6 and 7 present the empirical means and standard deviations calculated using DQMoM-IEM with $N = 3$ particles. Figures 6 shows rapid reaction between species A and B. The product R forms rapidly in the reaction zone. The side-product S forms more slowly, with most forming in the zone of high concentration of B and R near the jet inlet. Figure 7(c) shows a saddle point in the standard deviation near the inlets to the reactor. In the case of DQMoM-IEM with $N = 2$ particles, this manifests itself as an arc of zero standard deviation running along the path defined by the dashed line on Figure 7(c) [2]. The use of $N = 3$ particles offers significant improvement in the resolution of the standard deviation in this region and is responsible for a small improvement in the agreement between the predicted and the experimental yields as per Table 3.

Table 3: *DQMoM-IEM reaction yields.*

Grid	DQMoM-IEM yield (%)			Literature yield data (%)	
	$N=2$ [a]	$N=2$ [b]	$N=3$ [b]	Transported PDF [c]	Expt. [d]
Base	80.4	80.7	81.9 [e]	81.0	82.1
Coarse	80.1	–	–	–	–
3D coarse	80.3	–	–	–	–

[a] *Analytic solver [2],* [b] *General solver [2],* [c] *Tsai and Fox [40, Table 3],* [d] *Li and Toor [28, Table 1],* [e] *See Figures 6 and 7.*

Figures 8 and 9 present the empirical means and standard deviations for a typical SF case with antithetic sampling. There are still some artifacts due to fluctuations, particularly in the mean of species R and S, see Figure 8(c) and (d). The sub-grid segregation is not fully resolved in the region between the inlets. This results in a significant concentration of the product R adjacent to the wall between the inlets on Figure 8(c). It is also evident in the lower values of the SF standard deviations reported for species A, B and S in Figures 9(a), (b) and (d), and the over-prediction of the standard deviation of species R in Figure 9(c).

Figure 10 plots the fluctuation of the yield at the reactor outlet for SF cases with $N = 4, 8, 16, 32, 64$ fields. The yield Y is calculated using equation (31) where

$$C_\alpha = \frac{\rho}{W_\alpha} \left\langle \phi_\alpha \right\rangle_N \Big|_{\text{reactor outlet}} . \tag{37}$$

The fluctuation is calculated as the difference between the maximum and minimum yields

$$\max_{t\in[1,5]\,\mathrm{s}} \left(Y\right) - \min_{t\in[1,5]\,\mathrm{s}} \left(Y\right), \tag{38}$$

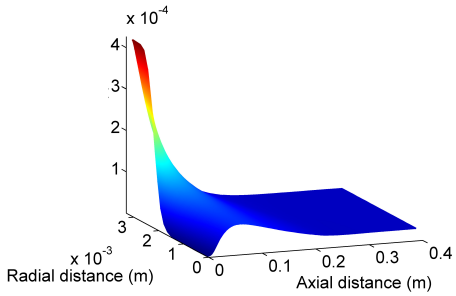

(a) *Empirical mean, species A.*

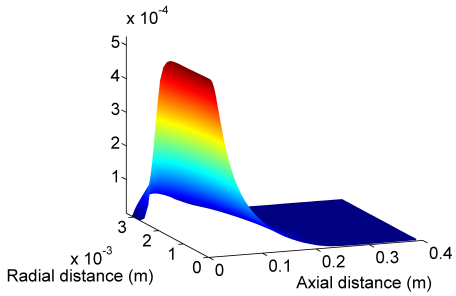

(b) *Empirical mean, species B.*

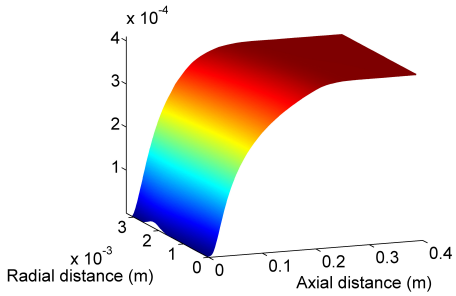

(c) *Empirical mean, species R.*

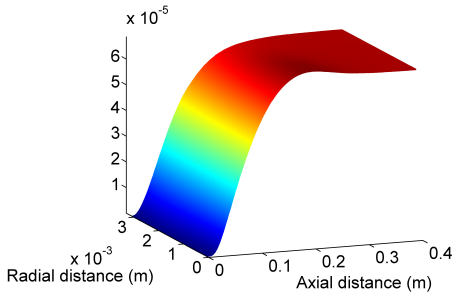

(d) *Empirical mean, species S.*

Figure 6: *Jet reactor empirical means for the reacting case on the base grid, DQMoM-IEM general solver with $N = 3$ particles.*

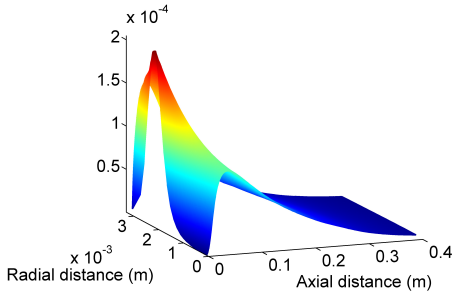

(a) *Empirical standard deviation, species A.*

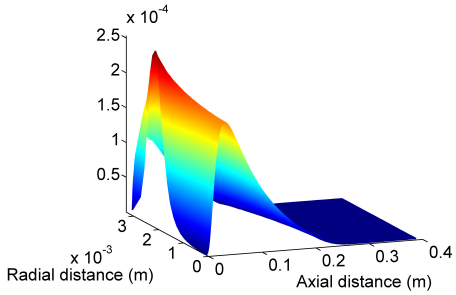

(b) *Empirical standard deviation, species B.*

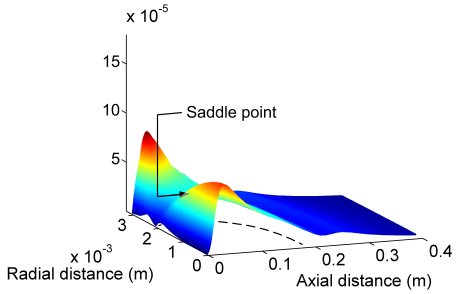

(c) *Empirical standard deviation, species R.*

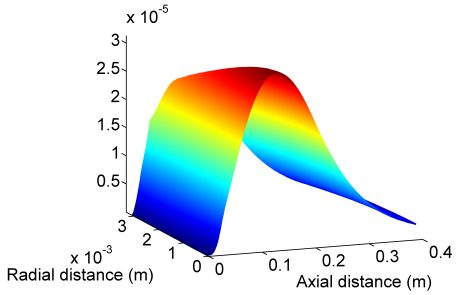

(d) *Empirical standard deviation, species S.*

Figure 7: *Jet reactor empirical standard deviations for the reacting case on the base grid, DQMoM-IEM general solver with $N = 3$ particles.*

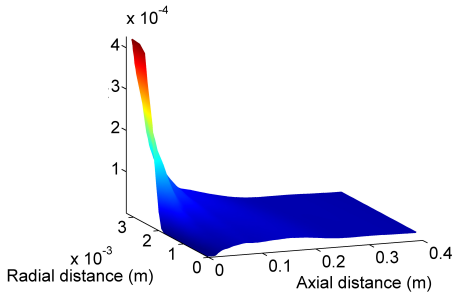

(a) *Empirical mean, species A.*

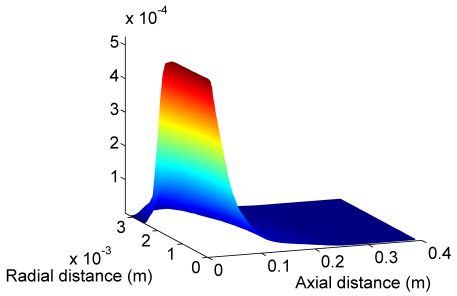

(b) *Empirical mean, species B.*

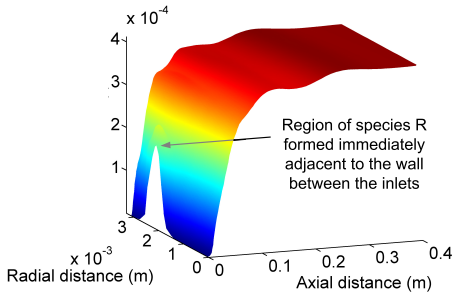

(c) *Empirical mean, species R.*

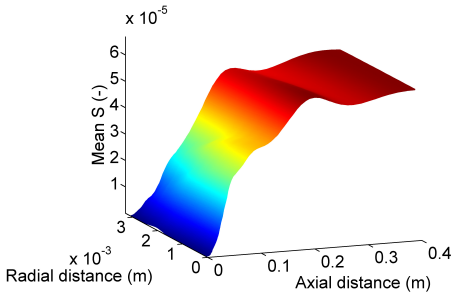

(d) *Empirical mean, species S.*

Figure 8: *Jet reactor empirical means for the reacting case at $t = 5$ s on the base grid, SF solver with antithetic sampling and $N = 64$ fields.*

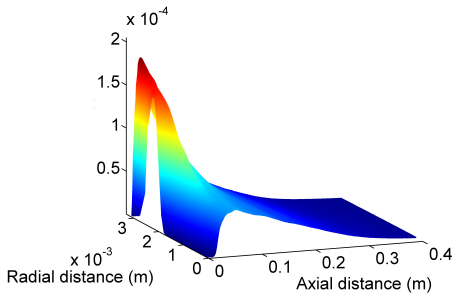

(a) *Empirical standard deviation, species A.*

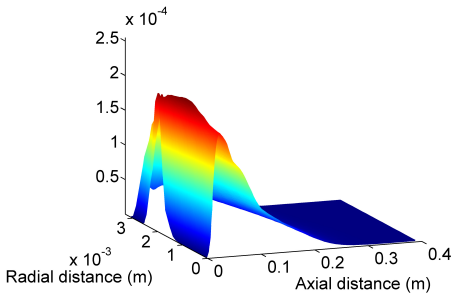

(b) *Empirical standard deviation, species B.*

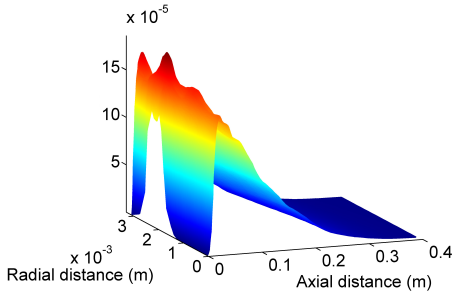

(c) *Empirical standard deviation, species R.*

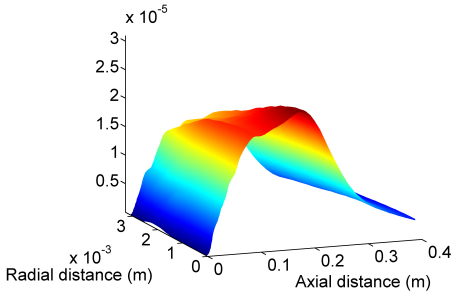

(d) *Empirical standard deviation, species S.*

Figure 9: *Jet reactor empirical standard deviations for the reacting case at $t = 5$ s on the base grid, SF solver with antithetic sampling and $N = 64$ fields.*

and shows analogous behaviour to Figure 4, with convergence at a rate proportional to $N^{-1/2}$ and clearly reduced fluctuations for the antithetic case on the base and coarse grids.

Figure 11 plots the SF time-averaged yield and the loci of the maximum and minimum yields at the reactor outlet, as defined by equations (31), (37) and (38). The yields converge to values slightly higher than for DQMoM-IEM and are estimated as $84-86\%$ for the base grid and $86-88\%$ for the coarse grids. The difference from DQMoM-IEM is due to the failure to fully resolve the sub-grid segregation near the reactor inlets. It can be shown that DQMoM-IEM reproduces an 85% yield when using the boundary conditions previously shown to reproduce the SF behaviour in Section 4.2. The differences between the SF cases on the base and coarse grids are due to how far each resolves the sub-grid segregation, as per the minor grid dependence identified in relation to Figure 5. In this example, DQMoM-IEM achieves a grid-independent solution more easily than SF. What defines an acceptable level of grid-independence will of course be application specific.

The difference between the standard and antithetic case loci of the maximum and minimum yields (marked by the gray areas on Figure 11) illustrate a clear benefit from the application of antithetic sampling to the base and coarse grids: a better estimate of the yield can be achieved with fewer particles. The data for the coarse 3D grid are consistent with, but no better than the standard case on the coarse grid.

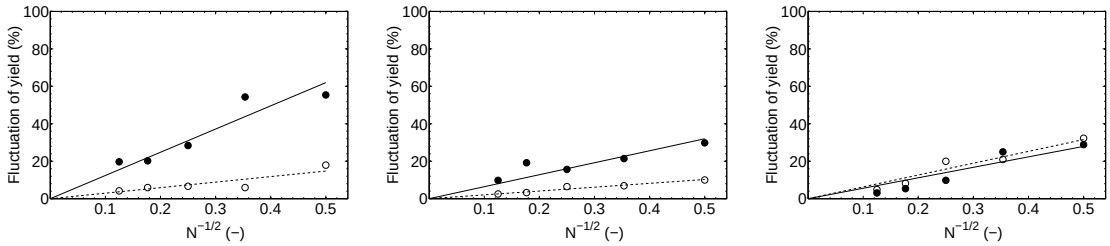

(a) *Base grid.* **(b)** *Coarse grid.* **(c)** *Coarse 3D grid.*

Figure 10: *Fluctuation of the SF yield at the jet reactor outlet for the reacting case in the interval $t \in [1,5]$ s. Solid symbols: standard case; Solid line: standard case guide line; Hollow symbols: antithetic case; Dashed line: antithetic case guide line.*

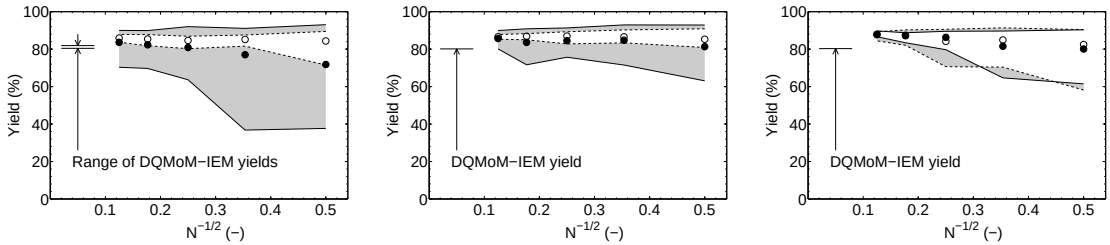

(a) *Base grid.* **(b)** *Coarse grid.* **(c)** *Coarse 3D grid.*

Figure 11: *SF yield at the jet reactor outlet for the reacting case in the interval $t \in [1,5]$ s. Solid symbols: standard case time-averaged yield; Solid line: standard case loci of maximum and minimum yields; Hollow symbols: antithetic case time-averaged yield; Dashed line: antithetic case loci of maximum and minimum yields. Shaded area: difference between standard and antithetic case loci of maximum and minimum yields.*

5 Conclusions

The performance of DQMoM-IEM and SF has been investigated for an axisymmetric turbulent reaction test case known from the literature. Cases have been considered on two grids that enforce an axisymmetric solution and on a 3D grid that resolves the full domain in a cartesian coordinate system. Equivalent predictions of the yields were demonstrated between the axisymmetric and 3D cases. DQMoM-IEM showed excellent agreement with experimental and transported PDF data. The SF method gave similar results, but retained a minor grid-dependence not seen with DQMoM-IEM. It did not fully resolve the sub-grid segregation of the species mass fractions, resulting in a systematic over-prediction of the yield. The prediction improved as the grid was refined, and could possibly be eliminated given sufficient refinement.

The SF cases showed significant variance in the solution. The expected convergence was demonstrated in the non-reacting case for fluctuations of the species mass fractions at the reactor outlet and for convergence of the full domain against the method of moments. In the reacting case, convergence was demonstrated for fluctuations of the yield. Antithetic variates were shown to increase statistical efficiency on the axisymmetric grids, enabling better convergence to be achieved with fewer particles. The situation for the 3D grid was less clear. The extra dimension bought improved efficiency at greater computational cost for the standard case, but eliminated much of the benefit from the antithetic case. It is believed that this is a consequence of solving the case in cartesian coordinates, and that an equivalent 3D case solved in cylindrical polar coordinates would reproduce the observations from the axisymmetric grids.

Antithetic variates are suggested as a simple way to increase the efficiency of the SF method. The example in this paper has demonstrated an axisymmetric formulation that accesses the benefits of both antithetic sampling and reduced dimensionality. The example has also highlighted areas where DQMoM-IEM offers some advantages. DQMoM-IEM was more easily able to achieve a grid-independent solution and gave a deterministic and accurate prediction of the yield with as few as $N = 2$ particles. The investigation of whether antithetic sampling offers benefits to the application of SF to problems in other geometries remains an important area of future research.

Acknowledgements

The authors thank reSolutions Ltd. and the EPSRC (EP/C537564/1) for financial support of Jethro Akroyd, and Dr Simon Lo of CD-adapco for licences and technical support.

Nomenclature

Upper-case Roman

C_α	Molar concentration of species α
C_ϕ	IEM micromixing model constant
K	Number of scalars
M	Number of moments
N	Number of particles / fields
Re	Reynolds number
$S_{\Delta t}$	Solution operator for an evolution equation
$S(\phi)$	Chemical source term vector
$U(x,t)$	Eulerian velocity vector
W	Wiener process, see Gardiner [10]
W_α	Relative molecular mass of scalar α
Y	Yield of the test reaction, see Eq. (31)
Y_α	Mass fraction of scalar α

Lower-case Roman

$a^{(n)}$	Source term for the weights $w^{(n)}$, see Eq. (4)
$b_\alpha^{(n)}$	Source term for the weighted positions $s_\alpha^{(n)}$, see Eq. (5)
$c_{\alpha\beta}^{(n)}$	Turbulent diffusion-spatial gradient term, see Eq. (13)
$f_\phi(\psi;x,t)$	Joint composition PDF of $\phi(x,t)$
k_1	Rate constant for the test reaction, see Eq. (30)
k_2	Rate constant for the test reaction, see Eq. (30)
m_α	Moment order of scalar α
$m_{\lambda\alpha}$	Moment order of scalar α in the λ^{th} empirical moment of the DQMoM-IEM particle system, see Eq. (7)
$s_\alpha^{(n)}$	Weighted particle position, see Eq. (6)
t	Time
$u(x,t)$	Fluctuating velocity field $u = U - \langle U \rangle$
$w^{(n)}$	Weight of particle n, see Eq. (2)
x	Position vector

Upper-case Greek

Γ_{T}	Turbulent diffusivity
Γ_α	Thermal diffusivity of scalar α

Lower-case Greek

$\delta_{\psi_\alpha^{(n)};x,t}$	Dirac delta function, see Eq. (3)
$\delta'_{\psi_\alpha^{(n)};x,t}$	First derivative of $\delta_{\psi_\alpha^{(n)};x,t}$
ϵ_{mean}	Convergence metric for the empirical mean, see Eq. (35)

ϵ_{sd}	Convergence metric for the empirical standard deviation, see Eq. (36)
ν_{T}	Turbulent viscosity
$\xi_i^{(n)}$	SF variate relating to direction i and field n
ρ	Density
σ_{T}	Turbulent Schmidt number
τ_ϕ	IEM micromixing model mixing time
$\phi(x,t)$	Eulerian passive scalar (composition) vector
ψ	Sample space variable corresponding to ϕ
$\psi_\alpha^{(n)}$	Value of scalar α on particle / field n, see Eqs. (2) and (14)

Superscripts

(n)	Denotes the n^{th} particle

Subscripts

dx	Denotes the diffusion term
mx	Denotes the micromixing term
rx	Denotes the reaction term
i	Denotes the i^{th} direction
α	Denotes the α^{th} scalar
β	Denotes the β^{th} scalar
γ	Denotes the γ^{th} scalar
λ	Denotes the λ^{th} moment

Symbols

$\langle \quad \rangle$	Expectation
$\langle \cdot \vert \psi \rangle$	Expectation conditioned on $\phi = \psi$
$\langle \quad \rangle_N$	Empirical expectation over N particles
$\langle \phi_\alpha \rangle_N$	Empirical mean of ϕ_α over N particles
$\langle \phi_\alpha^2 \rangle_N$	Empirical second moment of ϕ_α over N particles

Abbreviations

CFD	Computational fluid dynamics
DQMoM	Direct quadrature method of moments
IEM	Interaction by exchange with the mean
PDF	Probability density function
RANS	Reynolds-averaged Navier-Stokes
SF	Stochastic Fields method
SPDE	Stochastic partial differential equation

References

[1] J. H. Ahrens and U. Dieter. Extensions of Forsythe's method for random sampling from the normal distribution. *Mathematics of Computation*, 27(124):927–937, 1973.

[2] J. Akroyd, A. Smith, L. R. McGlashan, and M. Kraft. Numerical investigation of DQMoM-IEM as a turbulent reaction closure. *Chemical Engineering Science*, 65 (6):1915–1924, 2010. doi:10.1016/j.ces.2009.11.010.

[3] A. Bhave and M. Kraft. Partially stirred reactor model: Analytical solutions and numerical convergence study of a PDF/Monte Carlo method. *SIAM Journal on Scientific Computing*, 25(5):1798–1823, 2004. doi:10.1137/S1064827502411328.

[4] P. Boyle, M. Brodie, and P. Glassernan. Monte Carlo methods for security pricing. *Journal of Economic Dynamics and Control*, 21(8-9):1267–1321, 1997. doi:10.1016/S0165-1889(97)00028-6.

[5] CD-adapco. Star-CD v4.08.006, 2008. URL `http://www.cd-adapco.com/`.

[6] R. C. H. Cheng. The use of antithetic variates in computer simulations. *Journal of the Operational Research Society*, 33(3):229–237, 1982. URL `http://www.jstor.org/stable/2581487`.

[7] G. S. Fishman. *Monte Carlo: Concepts, Algorithms and Applications*. Springer-Verlag, New York, 1996.

[8] G. S. Fishman and B. D. Huang. Antithetic variates revisited. *Communications of the ACM*, 26(11):964 – 971, 1983. doi:10.1145/182.358462.

[9] R. O. Fox. *Computational Models for Turbulent Reacting Flows*. Cambridge University Press, Cambridge, 2003.

[10] C. W. Gardiner. *Handbook of Stochastic Methods*. Springer, Berlin, 3rd edition, 2004.

[11] A. Garmory. *Micromixing Effects in Atmospheric Reacting Flows*. PhD thesis, University of Cambridge, 2007.

[12] A. Garmory, E. S. Richardson, and E. Mastorakos. Micromixing effects in a reacting plume by the Stochastic Fields method. *Atmospheric Environment*, 40(6):1078–1091, 2006. doi:10.1016/j.atmosenv.2005.11.002.

[13] A. Garmory, I. S. Kim, R. E. Britter, and E. Mastorakos. Simulations of the dispersion of reactive pollutants in a street canyon, considering different chemical mechanisms and micromixing. *Atmospheric Environment*, page in press, 2008. doi:10.1016/j.atmosenv.2008.07.033.

[14] E. Gavi, D. L. Marchisio, and A. A. Baressi. CFD modelling and scale-up of confined impinging jet reactors. *Chemical Engineering Science*, 62(8):2228–2241, 2007. doi:10.1016/j.ces.2006.12.077.

[15] E. Gavi, L. Rivautella, D. L. Marchisio, M. Vanni, A. A. Baressi, and G. Baldi. CFD modelling of nano-particle precipitation in confined impinging jet reactors. *Chemical Engineering Research and Design*, 85(A5 Special Issue: 12th European Conference on Mixing):1–10, 2007. doi:10.1205/cherd06176.

[16] J. Geweke. Antithetic acceleration of Monte Carlo integration in Bayesian inference. *Jounral of Econometrics*, 38(1-2):73–89, 1988. doi:10.1016/0304-4076(88)90027-9.

[17] E. Hairer and G. Wanner. *Solving Ordinary Differential Equations II. Stiff and Differential-Algebraic Problems*, volume 14 of *Springer Series in Computational Mathematics*. Springer Verlag, Berlin, second revised edition, 1996.

[18] J. M. Hammersley and D. C. Handscomb. Proof of the antithetic variates theorem for $n > 2$. *Mathematical Proceedings of the Cambridge Philosophical Society*, 54 (2):300–301, 1958. doi:10.1017/S0305004100033454.

[19] J. M. Hammersley and J. G. Mauldon. General principles of antithetic variates. *Mathematical Proceedings of the Cambridge Philosophical Society*, 52(3):476–481, 1956. doi:10.1017/S0305004100031467.

[20] J. M. Hammersley and K. W. Morton. A new Monte Carlo technique: antithetic variates. *Mathematical Proceedings of the Cambridge Philosophical Society*, 52(3): 449–475, 1956. doi:10.1017/S0305004100031455.

[21] G. Hauke and L. Valiño. Computing reactive flows with a field Monte Carlo formulation and multi-scale methods. *Computer methods in applied mechanics and engineering*, 193(15-16):1455–1470, 2004. doi:10.1016/j.cma.2003.12.033.

[22] D. C. Haworth. Progress in probability density function methods for turbulent reacting flows. *Progress in Energy and Combustion Science*, in press, 2009. doi:10.1016/j.pecs.2009.09.003.

[23] W. P. Jones and S. Navarro-Martinez. Large eddy simulation of autoignition with a subgrid probability density function method. *Combustion and Flame*, 150(3):170–187, 2007. doi:10.1016/j.combustflame.2007.04.003.

[24] W. P. Jones and S. Navarro-Martinez. Numerical study of n-heptane auto-ignition using LES-PDF methods. *Flow, Turbulence and Combustion*, 83(3):407–423, 2009. doi:10.1007/s10494-009-9228-9.

[25] W. P. Jones, S. Navarro-Martinez, and O. Röhl. Large eddy simulation of hydrogen auto-ignition with a probability density function method. *Proceedings of the Combustion Institute*, 31(2):1765–1771, 2007. doi:10.1016/j.proci.2006.07.041.

[26] P. E. Kloeden and E. Platen. *Numerical Solution of Stochastic Differential Equations*. Springer, Berlin, second corrected printing edition, 1995.

[27] M. Kraft and H. Fey. Some analytic solutions for stochastic reactor models based on the joint composition PDF. *Combustion Theory and Modelling*, 3(2):343–358, 1999. doi:10.1088/1364-7830/3/2/308.

[28] K. T. Li and H. L. Toor. Turbulent reactive mixing with a series-parallel reaction: Effect of mixing on yield. *AIChE Journal*, 32(8):1312–1320, 1986. doi:10.1002/aic.690320809.

[29] P. A. Libby and F. A. Williams. *Turbulent Reacting Flows*. Springer, Berlin, 1980.

[30] Y. Lui and R. O. Fox. CFD predictions for chemical processing in a confined impinging-jets reactor. *AIChE Journal*, 52(2):731–744, 2006. doi:10.1002/aic.10633.

[31] M. Matsumoto and T. Nishimura. Mersenne Twister: A 623-dimensionally equidistributed uniform pseudo-random number generator. *ACM Transactions on Modeling and Computer Simulation*, 8(1):3–30, 1998.

[32] R. Mustata, L. Valiño, C. Jiménez, W. P. Jones, and S. Bondi. A probability density function Eulerian Monte Carlo field method for large eddy simulations: Application to a turbulent piloted methane/air diffusion flame (Sandia D). *Combustion and Flame*, 145(1-2):88–104, 2006. doi:10.1016/j.combustflame.2005.12.002.

[33] S. Paskov and J. Traub. Faster valuation of financial derivatives. *The Journal of Portfolio Management*, 22(1):113–123, 1995. doi:10.3905/jpm.1995.409541.

[34] N. Peters. *Turbulent Combustion*. Cambridge University Press, Cambridge, 2000.

[35] S. B. Pope. PDF methods for turbulent reacting flows. *Progress in Energy and Combustion Science*, 11(2):119–192, 1985. doi:10.1016/0360-1285(85)90002-4.

[36] V. Raman, H. Pitsch, and R. O. Fox. Eulerian transoprted probability denisty function sub-filter model for large-eddy simulations of turbulent combustion. *Combustion Theory and Modelling*, 10(3):439–548, 2006. doi:10.1080/13647830500460474.

[37] V. Sabel'nikov and O. Soulard. Rapidly decorrelating velocity-field model as a tool for solving one-point Fokker-Planck equations for probability density functions of turbulent reactive scalars. *Physical Review E*, 72(1):Article No. 016301, 2005. doi:10.1103/PhysRevE.72.016301.

[38] G. Strang. On the construction and comparison of difference schemes. *SIAM Journal on Numerical Analysis*, 5(3):506–517, 1968.

[39] Q. Tang, W. Zhao, M. Bockelie, and R. O. Fox. Multi-environment probability density function method for modelling turbulent combustion using realistic chemical kinetics. *Combustion Theory and Modelling*, 11(6):889–907, 2007. doi:10.1080/13647830701268890.

[40] K. Tsai and R. O. Fox. PDF simulation of a turbulent series-parallel reaction in an axisymmetric reactor. *Chemical Engineering Science*, 49(24B):5154–5158, 1994. doi:10.1016/0009-2509(94)00270-3.

[41] K. Tsai, P. A. Gillis, S. Sen, and R. O. Fox. A finite-mode PDF model for turbulent reacting flows. *Journal of Fluids Engineering*, 124(1):102–107, 2002. doi:10.1115/1.1431546.

[42] L. Valiño. A field Monte Carlo formulation for calculating the probability density function of a single scalar in a turbulent flow. *Flow, Turbulence and Combustion*, 60 (2):157–172, 1998. doi:10.1023/A:1009968902446.

[43] J. Villermaux and J. C. Devillon. Représentation de la coalescence et de la redispersion des domaines de ségrégation dans un fluide par un modèle d'interaction phénoménologique. In *Proceedings of the 2nd International Symposium on Chemical Reaction Engineering*, pages 1–13. International Symposium on Chemical Reaction Engineering, Elsevier, New York, 1972.

[44] L. Wang and R. O. Fox. Comparison of micromixing models for CFD simulation of nanoparticle formation. *AIChE Journal*, 50(9):2217–2232, 2004. doi:10.1002/aic.10173.

[45] J. R. Wilson. Proof of the antithetic-variates theorem for unbounded functions. *Mathematical Proceedings of the Cambridge Philosophical Society*, 86(03):477–479, 1979. doi:10.1017/S0305004100056334.

[46] J. R. Wilson. Antithetic sampling with multivariate inputs. *American Journal of Mathematical and Management Sciences*, 3:121–144, 1983.

Citation index

Ahrens and Dieter [1], 8
Akroyd et al. [2], 4–8, 10–12, 14, 15
Bhave and Kraft [3], 8
Boyle et al. [4], 9
CD-adapco [5], 7, 10
Cheng [6], 9
Fishman and Huang [8], 9
Fishman [7], 9
Fox [9], 3, 4
Gardiner [10], 6, 8, 20
Garmory et al. [12], 3
Garmory et al. [13], 3
Garmory [11], 8, 11
Gavi et al. [14], 3
Gavi et al. [15], 3, 14
Geweke [16], 9
Hairer and Wanner [17], 7
Hammersley and Handscomb [18], 9
Hammersley and Mauldon [19], 9
Hammersley and Morton [20], 9
Hauke and Valiño [21], 6
Haworth [22], 3
Jones and Navarro-Martinez [23], 3
Jones and Navarro-Martinez [24], 3
Jones et al. [25], 3
Kloeden and Platen [26], 8
Kraft and Fey [27], 8
Li and Toor [28], 3, 10, 15
Libby and Williams [29], 3
Lui and Fox [30], 3
Matsumoto and Nishimura [31], 8
Mustata et al. [32], 3
Paskov and Traub [33], 9
Peters [34], 3
Pope [35], 3
Raman et al. [36], 3
Sabel'nikov and Soulard [37], 3, 5, 11
Strang [38], 7, 8
Tang et al. [39], 3
Tsai and Fox [40], 3, 10, 15
Tsai et al. [41], 3
Valiño [42], 3, 5, 6
Villermaux and Devillon [43], 3
Wang and Fox [44], 3
Wilson [45], 9
Wilson [46], 9

A SF derivation

This section summarises the derivation of the Itô SPDE given by equation (15). This result was first given by Hauke and Valiño [21]. The derivation follows the approach outlined by Valiño [42] and requires that the fields are twice differentiable in space.

The derivation starts with a transport equation for the one-point one-time joint composition PDF f_ϕ [35]. This equation is exact and contains no approximations

$$\begin{aligned}\frac{\partial f_\phi}{\partial t} + \frac{\partial}{\partial x_i}\left(\left[\langle U_i\rangle + \langle u_i|\,\psi\rangle\right] f_\phi\right) = \\ -\frac{\partial}{\partial \psi_\alpha}\left(\left[\left\langle \Gamma_\alpha \nabla^2\phi_\alpha\right|\,\psi\right\rangle + S_\alpha(\psi)\right] f_\phi\right).\end{aligned} \tag{A.1}$$

The turbulent convective flux $f_\phi\,\langle u|\,\psi\rangle$ and molecular diffusion $\langle \Gamma_\alpha\nabla^2\phi_\alpha|\,\psi\rangle$ terms need to be closed. $S_\alpha(\psi)$ is the chemical source term. It describes the material and energy balance of species α and is closed.

Equation (A.1) is closed using a gradient diffusion model for the convective flux, and an IEM model to approximate the molecular diffusion [43]

$$-f_\phi\,\langle u|\,\psi\rangle = \Gamma_\mathrm{T}\nabla f_\phi\,, \tag{A.2}$$

$$\left\langle \Gamma_\alpha\nabla^2\phi_\alpha\right|\,\psi\rangle = \frac{C_\phi}{2\tau_\phi}\left(\langle\phi_\alpha\rangle - \psi_\alpha\right), \tag{A.3}$$

where C_ϕ is an empirical constant and τ_ϕ is the scalar mixing time. Equation (A.3) assumes that all scalars mix at the same rate. The turbulent diffusivity Γ_T is calculated

$$\Gamma_\mathrm{T} = \nu_\mathrm{T}/\sigma_\mathrm{T}\,, \tag{A.4}$$

where the turbulent viscosity ν_T is prescribed by the turbulence model and the turbulent Schmidt number σ_T is typically close to unity. The closed form of equation (A.1) appears in the main text as equation (1) and is written

$$\begin{aligned}\frac{\partial f_\phi}{\partial t} + \langle U_i\rangle\frac{\partial f_\phi}{\partial x_i} - \frac{\partial}{\partial x_i}\left(\Gamma_\mathrm{T}\frac{\partial f_\phi}{\partial x_i}\right) = \\ -\frac{\partial}{\partial \psi_\alpha}\left(\left[\frac{C_\phi}{2\tau_\phi}\left(\langle\phi_\alpha\rangle - \psi_\alpha\right) + S_\alpha(\psi)\right] f_\phi\right).\end{aligned} \tag{A.5}$$

The PDF in equation (A.5) evolves by **convection and diffusion** according to

$$\frac{\partial f_\phi}{\partial t} = -\langle U_i\rangle\frac{\partial f_\phi}{\partial x_i} + \frac{\partial}{\partial x_i}\left(\Gamma_\mathrm{T}\frac{\partial f_\phi}{\partial x_i}\right). \tag{A.6}$$

We substitute the stochastic field approximation given in the main text as equation (14)

$$\begin{aligned} f_\phi(\psi; x, t) &= f_\phi(\psi_1, \ldots, \psi_K; x, t) \\ &\approx \frac{1}{N} \sum_{n=1}^{N} \prod_{\alpha=1}^{K} \delta_{\psi_\alpha^{(n)}; x, t}\,, \end{aligned} \tag{A.7}$$

into equation (A.6) to give

$$\frac{\partial f_\phi}{\partial t} = \frac{1}{N} \sum_{n=1}^{N} \left[- \langle U_i \rangle \frac{\partial}{\partial x_i} \prod_{\alpha=1}^{K} \delta_{\psi_\alpha^{(n)}; x, t} + \frac{\partial}{\partial x_i} \left(\Gamma_{\mathrm{T}} \frac{\partial}{\partial x_i} \prod_{\alpha=1}^{K} \delta_{\psi_\alpha^{(n)}; x, t} \right) \right], \tag{A.8}$$

such that

$$\begin{aligned} \frac{\partial f_\phi}{\partial t} = \frac{1}{N} \sum_{n=1}^{N} \Bigg[& \sum_{\alpha=1}^{K} \frac{\partial}{\partial \psi_\alpha} \left(\langle U_i \rangle \frac{\partial \psi_\alpha^{(n)}}{\partial x_i} \prod_{\beta=1}^{K} \delta_{\psi_\beta^{(n)}} \right) \\ & - \sum_{\alpha=1}^{K} \frac{\partial}{\partial \psi_\alpha} \left(\frac{\partial}{\partial x_i} \left(\Gamma_{\mathrm{T}} \frac{\partial \psi_\alpha^{(n)}}{\partial x_i} \right) \prod_{\beta=1}^{K} \delta_{\psi_\beta^{(n)}} \right) \\ & + \sum_{\alpha=1}^{K} \sum_{\beta=1}^{K} \frac{\partial^2}{\partial \psi_\alpha \partial \psi_\beta} \left(\Gamma_{\mathrm{T}} \frac{\partial \psi_\alpha^{(n)}}{\partial x_i} \frac{\partial \psi_\beta^{(n)}}{\partial x_i} \prod_{\gamma=1}^{K} \delta_{\psi_\gamma^{(n)}} \right) \Bigg], \end{aligned} \tag{A.9}$$

where

$$\begin{aligned} \frac{\partial}{\partial x_i} \prod_{\alpha=1}^{K} \delta_{\psi_\alpha^{(n)}} &= - \sum_{\alpha=1}^{K} \frac{\partial \psi_\alpha^{(n)}}{\partial x_i} \delta'_{\psi_\alpha^{(n)}} \prod_{\substack{\beta=1 \\ \beta \neq \alpha}}^{K} \delta_{\psi_\beta^{(n)}} \\ &= - \sum_{\alpha=1}^{K} \frac{\partial}{\partial \psi_\alpha} \left(\frac{\partial \psi_\alpha^{(n)}}{\partial x_i} \prod_{\beta=1}^{K} \delta_{\psi_\beta^{(n)}} \right), \end{aligned} \tag{A.10}$$

and using equation (A.10)

$$\begin{aligned} \frac{\partial}{\partial x_i} \left(\Gamma_{\mathrm{T}} \frac{\partial}{\partial x_i} \prod_{\alpha=1}^{K} \delta_{\psi_\alpha^{(n)}} \right) &= - \sum_{\alpha=1}^{K} \frac{\partial}{\partial \psi_\alpha} \frac{\partial}{\partial x_i} \left(\Gamma_{\mathrm{T}} \frac{\partial \psi_\alpha^{(n)}}{\partial x_i} \prod_{\beta=1}^{K} \delta_{\psi_\beta^{(n)}} \right) \\ &= - \sum_{\alpha=1}^{K} \frac{\partial}{\partial \psi_\alpha} \left(\frac{\partial}{\partial x_i} \left(\Gamma_{\mathrm{T}} \frac{\partial \psi_\alpha^{(n)}}{\partial x_i} \right) \prod_{\beta=1}^{K} \delta_{\psi_\beta^{(n)}} \right) \\ &\quad + \sum_{\alpha=1}^{K} \sum_{\beta=1}^{K} \frac{\partial^2}{\partial \psi_\alpha \partial \psi_\beta} \left(\Gamma_{\mathrm{T}} \frac{\partial \psi_\alpha^{(n)}}{\partial x_i} \frac{\partial \psi_\beta^{(n)}}{\partial x_i} \prod_{\gamma=1}^{K} \delta_{\psi_\gamma^{(n)}} \right). \end{aligned} \tag{A.11}$$

Equation (A.9) is a Fokker-Planck equation in time-composition space and has an equivalent SPDE [10] describing the contribution to each field

$$\mathrm{d}\psi_\alpha^{(n)} = -\langle U_i \rangle \frac{\partial \psi_\alpha^{(n)}}{\partial x_i}\,\mathrm{d}t + \frac{\partial}{\partial x_i}\left(\Gamma_\mathrm{T}\frac{\partial \psi_\alpha^{(n)}}{\partial x_i}\right)\mathrm{d}t + \left(2\Gamma_\mathrm{T}\right)^{1/2}\frac{\partial \psi_\alpha^{(n)}}{\partial x_i}\,\mathrm{d}W_i^{(n)}\,. \tag{A.12}$$

Likewise, the **micromixing and reaction terms** in equation (A.5)

$$\frac{\partial f_\phi}{\partial t} = -\frac{\partial}{\partial \psi_\alpha}\left(\frac{C_\phi}{2\tau_\phi}\big(\langle \phi_\alpha \rangle - \psi_\alpha\big) f_\phi\right) - \frac{\partial}{\partial \psi_\alpha}\Big(S_\alpha\big(\psi\big) f_\phi\Big)\,, \tag{A.13}$$

imply the following contributions to each field

$$\mathrm{d}\psi_\alpha^{(n)} = \frac{C_\phi}{2\tau_\phi}\Big(\langle \phi_\alpha \rangle_N - \psi_\alpha^{(n)}\Big)\,\mathrm{d}t + S_\alpha\Big(\psi^{(n)}\Big)\,\mathrm{d}t\,. \tag{A.14}$$

The **total contribution** to each field is given by the sum of equations (A.12) and (A.14)

$$\begin{aligned}\mathrm{d}\psi_\alpha^{(n)} = &-\langle U_i \rangle \frac{\partial \psi_\alpha^{(n)}}{\partial x_i}\,\mathrm{d}t + \frac{\partial}{\partial x_i}\left(\Gamma_\mathrm{T}\frac{\partial \psi_\alpha^{(n)}}{\partial x_i}\right)\mathrm{d}t \\ &+ \frac{C_\phi}{2\tau_\phi}\Big(\langle \phi_\alpha \rangle_N - \psi_\alpha^{(n)}\Big)\,\mathrm{d}t + S_\alpha\Big(\psi^{(n)}\Big)\,\mathrm{d}t \\ &+ \left(2\Gamma_\mathrm{T}\right)^{1/2}\frac{\partial \psi_\alpha^{(n)}}{\partial x_i}\,\mathrm{d}W_i^{(n)}\,.\end{aligned} \tag{A.15}$$

This is the result given by Hauke and Valiño [21] and is equation (15) in the main text.